IIETA International Information and Engineering Technology Association
Advancing the World of Information and Engineering

Mathematical Modelling of Engineering Problems
Vol. 12, No. 2, February, 2025, pp. 434-442
Journal homepage: http://iieta.org/journals/mmep

Numerical Investigation of Diffuser-Shaped Vortex Generators with Semi-Open Angles on Cylindrical Towers

Anan Sudsanguan[1], Amnart Boonloi[2], Withada Jedsadaratanachai[1*]

[1] Department of Mechanical Engineering, School of Engineering, King Mongkut's Institute of Technology Ladkrabang, Bangkok 10520, Thailand
[2] Department of Mechanical Engineering Technology, College of Industrial Technology, King Mongkut's University of Technology North Bangkok, Bangkok 10800, Thailand

Corresponding Author Email: withada.je@kmitl.ac.th

https://doi.org/10.18280/mmep.120208

Received: 2 December 2024
Revised: 19 January 2025
Accepted: 24 January 2025
Available online: 28 February 2025

Keywords:
wind solar tower, wind energy, solar updraft tower, turbulence modeling, diffuser-shaped chimney

ABSTRACT

This study presents a numerical investigation into the flow configurations and pressure distribution of cylindrical towers equipped with various vortex generators. The primary objective is to reduce the energy consumption of ventilation in these towers. Different diffuser-shaped vortex generators with semi-open angles are compared to determine the optimal angle for generating an upward suction draft. The study also examines the effects of air velocity and vortex generator size on flow configuration. The finite element method, implemented through commercial software, is employed to solve the main problem. The numerical results reveal that the suction draft speed within the tower is directly proportional to the crosswind speed. The diffuser-shaped vortex generator with a height equivalent to 2D provides the most effective ventilation. Furthermore, a semi-open angle of 8° proves to be the most suitable for cylindrical towers, with increasing semi-open angles resulting in enhanced updraft wind speeds.

1. INTRODUCTION

Currently, solar updraft towers are being continuously developed with the aim of increasing the speed of updraft airflow, thereby enhancing the electricity generation capacity of turbines. A concept has been proposed to harness upper wind energy to boost electricity production during nighttime, enabling the tower to generate power continuously throughout the day by utilizing crosswind energy. The operational mechanism of industrial ventilation stacks resembles that of solar updraft towers. However, ventilation stacks rely on exhaust fans to expel hot air or gases from industrial processes through the stack outlet, a process referred to as a ventilation system. Each year, a significant amount of energy is consumed to support these ventilation processes.

The development of solar updraft towers offers a promising approach for utilizing crosswind energy to reduce the energy consumption of ventilation systems. The original concept of solar updraft towers was validated by Haaf et al. [1, 2], and numerous studies have since investigated the effects of crosswind on these towers. Prtetorius and Kröger [3], along with Ming et al. [4] and Shen et al. [5], emphasized the potential of strong winds to enhance the driving force of these towers. Numerical studies [6-8] have further supported this hypothesis. Additionally, Ohya et al. [9] and Ridwan et al. [10] developed diffuser-shaped chimneys to increase the updraft velocity, with their findings aligning with this concept. Nevertheless, designing diffuser-shaped towers for solar updraft applications requires careful consideration of structural integrity. Most existing towers feature a cylindrical design, which poses challenges for structural modifications. As such, advancing solar updraft towers while retaining the original cylindrical structure represents a practical and appealing direction for future development.

An interesting approach for practical implementation is the development and installation of devices on existing tower structures. Several studies have explored similar strategies by installing equipment designed to harness the benefits of crosswind flows. The application of diffuser-shaped designs has been developed to enhance wind turbine performance, particularly through their integration into Wind-Lens systems [11-15]. These designs effectively increase wind speed passing through the turbines. Additionally, the diffuser shape generates vortex flows, consistent with the findings of references [16, 17], which highlight the potential of devices for converting crosswinds into vortex flows. This research approach underscores that installing equipment without altering the original structure is an appealing and practical strategy for real-world applications.

Watanabe et al. [18] investigated the utilization of crosswind to enhance updraft velocity by installing one-directional flat vortex generators of varying heights at the tower outlet. Their results demonstrated that vortex generators can effectively convert crosswind into vortex flows, thereby increasing updraft speed. Subsequent studies [19, 20] further explored three-directional vortex generators to identify the optimal design. These findings revealed that diffuser-shaped vortex generators offer the greatest potential for development.

The objective of this research is to increase the updraft velocity of the tower by utilizing crosswinds to enhance the suction power of a cylindrical-shaped tower. This is achieved by installing vortex generators at the top of the tower, an advancement over the original concept that used flat plates installed only on one side of the tower inlet. This modification improves the feasibility of real-world installation and allows the tower to capture wind from all directions.

In this study, wind-catching plates in three directions, as shown in Figure 1, are used. Based on previous studies [18, 19, 20], diffuser shapes are considered promising for the development of vortex generators. To test this hypothesis, diffuser-shaped vortex generators were constructed and tested at various half-open angles. The experimental results from [18] were used to validate the numerical simulations. This concept would enable the solar updraft tower to harness wind energy, allowing it to operate continuously both day and night while reducing energy consumption for industrial ventilation.

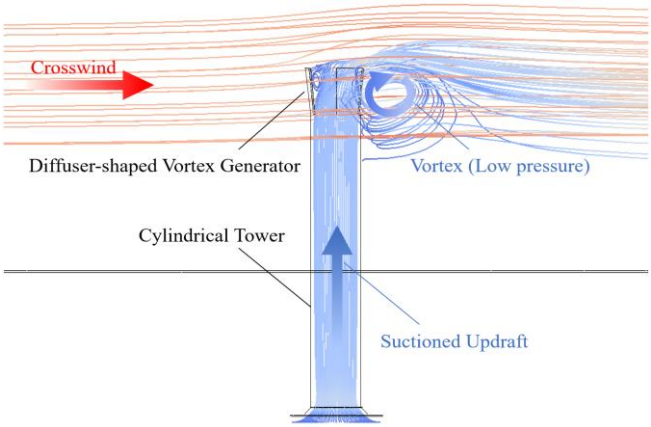

Figure 1. Working principle of a diffuser-shaped vortex generator on a cylindrical tower

2. NUMERICAL MODELS AND SETTING

In this study, the pressure coefficient (C_p) was designated by Eq. (1). The resulting value was obtained by dividing the static pressure difference by the dynamic pressure of the nearest wind approaching the tower.

$$C_p = \frac{\Delta p_s}{(1/2)\rho U_\infty^2} \tag{1}$$

The equation was simplified as:

$$C_p = \frac{p - p_\infty}{(1/2)\rho U_\infty^2} \tag{2}$$

In both equations, U_∞ means the velocity of the fluid (m.s^{-1}), while p means static pressure at a pressure coefficient assessment point (kg.m^{-2}), and p_∞ means static pressure of a freestream (kg.m^{-2}).

Commercial fluid analysis software (Ansys-Fluent) was utilized in this study to develop the numerical model of the experiments. The computational domain, as depicted in Figure 2, and the computational grid, shown in Figure 3, were replicated from the wind tunnel experiments. The computational domain encompassed not only the upper part where the wind typically flows but also the base on the leeward side, as evidenced by the tetrahedral-shaped structures in the computational grid. The model simulated the wind flow pattern within the cylindrical tower, with air velocities controlled at 2, 4, 6, and 8 m/s. The figure designation referred to Watanabe et al. [18] for accuracy.

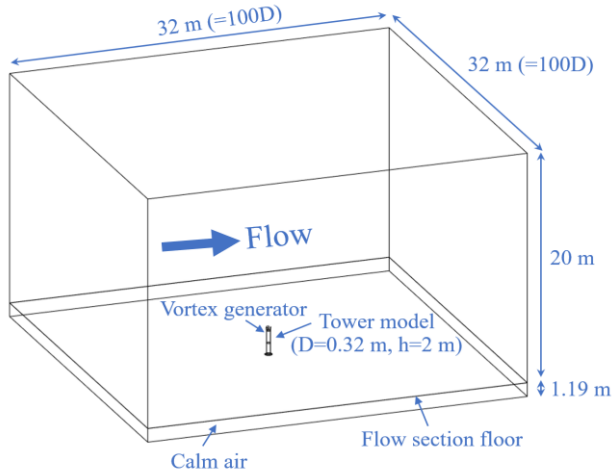

Figure 2. The computational domain

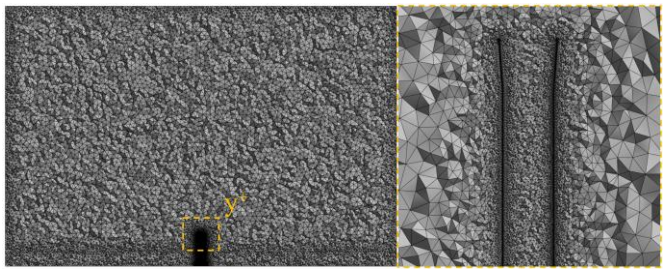

Figure 3. The computational grid

In the numerical model, turbulence kinetic energy (k) can be written in Launder and Spalding's [21] Standard k-epsilon Turbulence Model as in Eq. (3):

$$\frac{\partial}{\partial t}(\rho k) + \frac{\partial}{\partial x_i}(\rho k u_i) = \frac{\partial}{\partial x_j}\left[\left(\mu + \frac{\mu_t}{\sigma_k}\right)\frac{\partial k}{\partial x_j}\right] + P_k + P_b - \rho\varepsilon + S_k \tag{3}$$

A decrease in the specific kinetic energy dissipation rate (ε) was shown in Eq. (4):

$$\frac{\partial}{\partial t}(\rho\varepsilon) + \frac{\partial}{\partial x_i}(\rho\varepsilon u_i) = \frac{\partial}{\partial x_j}\left[\left(\mu + \frac{\mu_t}{\sigma_\varepsilon}\right)\frac{\partial \varepsilon}{\partial x_j}\right] + C_{1\varepsilon}\frac{\varepsilon}{k}\left(P_k + C_{3\varepsilon}P_b\right) - C_{2\varepsilon}\rho\frac{\varepsilon^2}{k} + S_\varepsilon \tag{4}$$

In both equations, k means specific turbulent kinetic energy (m^2.s^{-2}), μ_t means Eddy viscosity (kg.m^{-1}.s^{-1}), p means fluid density (kg.m^{-3}), μ_i means fluid freestream velocity (m.s^{-1}), σ_k, σ_ε, $C_{1\varepsilon}$ and $C_{2\varepsilon}$ are Standard k-epsilon Turbulence Model constant, and ε the specific kinetic energy dissipation rate (m^2.s^{-3}).

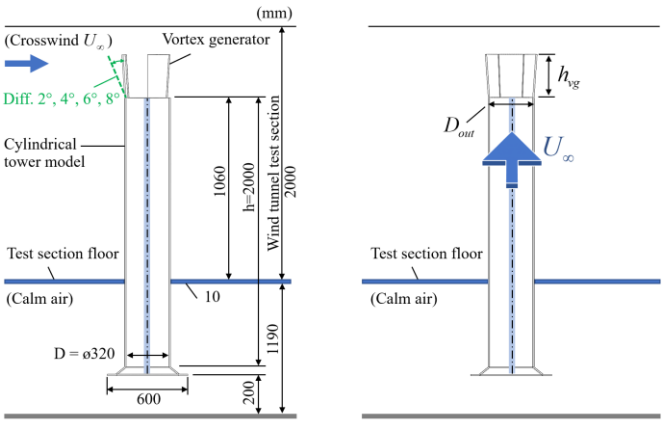

Figure 4. General conditions of the wind tunnel experiment

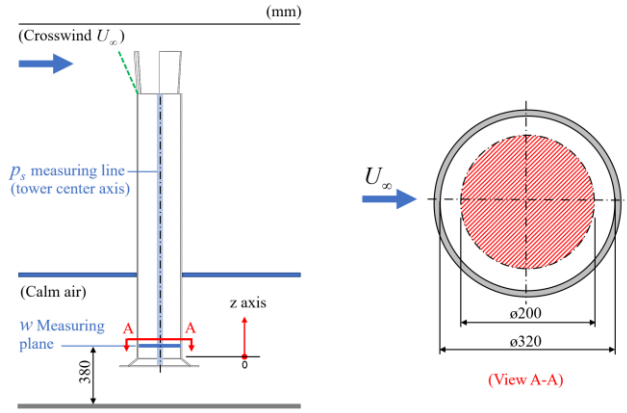

Figure 5. A cross-sectional area used to measure an over-the-top wind and static pressure

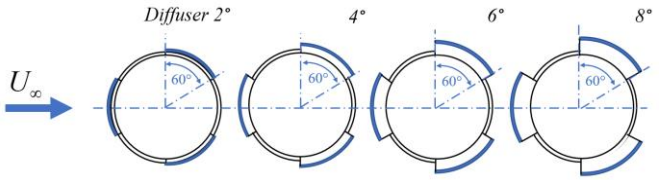

Figure 6. Width of diffuser-shaped vortex generators used in the numerical model

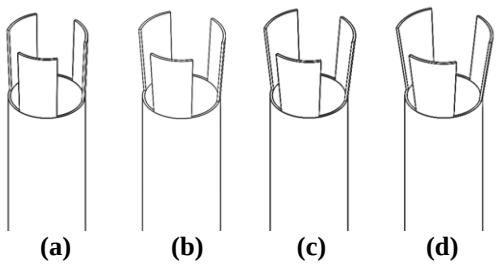

Figure 7. Diffuser-shaped vortex generators used in the numerical setting: (a) 2° Diffuser-shaped vortex generator; (b) 4° Diffuser-shaped vortex generator; (c) 6° Diffuser-shaped vortex generator; (d) 8° Diffuser-shaped vortex generator

The cylindrical-shaped tower is defined with a diameter *D* of 0.32 m and a height h of 2.0 m, as shown in Figure 4. The area used for measuring updraft velocity and pressure coefficients is shown in Figure 5, with the width of the tower inlet set to $D_{out} = D$. All generators used in this study were designed with three wind plates with the generator heights (h_{vg}) used in this study at *D/2*, *D* and *2D* respectively, and had a width of D/2 or 60° from the outlet center line in radius, as seen in Figure 6. All of the wind plates were constructed in a semi-open angle format, angled at 2°, 4°, 6°, and 8°, as shown in Figure 7. Air properties were defined at a temperature of 20 °C, with a thermal conductivity of 0.02514 W/m·K and specific heat of 1007 J/kg·K. Standard k-epsilon Turbulence Model are $\sigma_k = 1$, $\sigma_\varepsilon = 1.3$, $C_{1\varepsilon} = 1.44$, $C_{2\varepsilon} = 1.92$ and $C_\mu = 0.09$.

3. RESULTS AND DISCUSSION

3.1 Numerical models validation

Referring to the results conducted by Watanabe et al. [18], which were obtained by comparing data from actual experiments with those generated by fluid analysis software, this study utilized this dataset to validate the reliability of the numerical model. The experiment [18] involved the use of a single-plated vortex generator with the same width as the tower outlet. Consequently, the numerical model developed in this study aimed to replicate conditions as closely as possible to the actual experiment for enhanced reliability of the results.

The validation was aimed at validating the Turbulence Model used in this study, and designate conditions for the computational domain. The validation also looked at the suitable computational mesh based on its element quality, skewness, and orthogonal quality. A suitable wall function designation that led to the least convergence problems of the results processed by the Standard k-epsilon Turbulence Model possible [22-26] was also under inspection. The results from the simulation of the optimal node size, conducted for a cylindrical tower without vortex generators, are shown in Figure 8. This figure illustrates the relationship between wind speed and node density. The study found that increasing the number of nodes from 3.00E+06 to 5.50E+06 did not significantly affect the wind speed. Therefore, a numerical model was developed using approximately 3.00E+06 nodes for all cases under investigation.

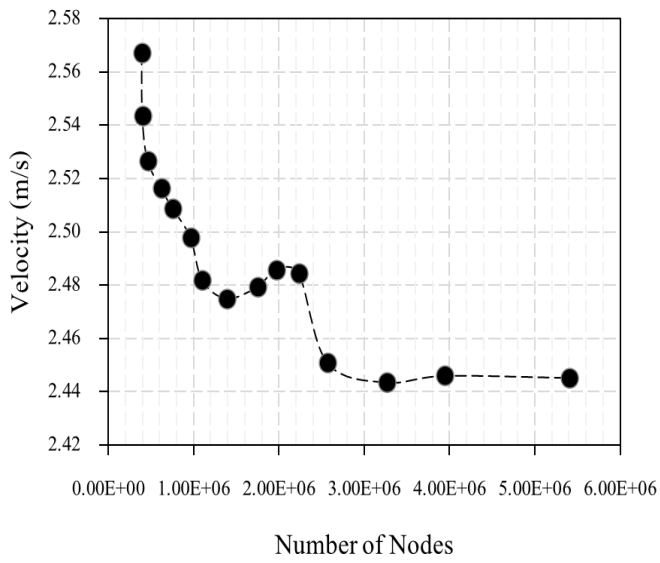

Figure 8. Number of nodes used to achieve optimum mesh

Results from the Standard k-epsilon Turbulence Model equation was displayed in Figure 9. Compared with the results processed by the Large Eddy Simulation (LES) from Watanabe et al. [18], it showed that the most usable set of data for the comparison of the results is the set collected on the tower without the vortex generator, shown in black circle-lined shape symbols in the graph. A fit curve of the trend line of the actual experiment was at $0.397U_{\infty}$, while a fit curve from the calculation based on the LES Turbulence Model (shown in yellow circle-lined shape symbols in the graph) by Watanabe et al. [18] and the results in this numerical model that used the Standard k-epsilon Turbulence Model (shown in black colored shape symbols in the graph) was at $0.316U_{\infty}$. Regarding an updraft windspeed, the validation provided a similar relationship between the velocity and the height of wind plates as an actual experiment, even though it provided a lower wind speed than an actual experiment. When comparing an updraft windspeed increasing ratio between the tower without the vortex generator and the tower with the *D/2* height vortex generator, numerical results showed that the updraft windspeed increasing rate both in the numerical model and the actual experiment had only a 2% difference. This can be said that the numerical model used in this study was considered reliable to use with the fluid analysis on the different vortex generators, and aimed at calculating final results and the fluidity increasing ratio assessment. When comparing with the pressure coefficient shown in Figure 10, it can be said that the pressure of the cylindrical tower without the generator and the tower with the *D/2* height vortex generator had a similar decreasing ratio as the results process from the LES turbulence model and the actual experiment by Watanabe et al. [18]. The results led to the designation of the calculation domain and the grid schematics used to design a numerical simulator of the semi-open angle diffuser-shaped vortex generator without actually constructing it as a costly experiment, which was more suitable for this study's condition.

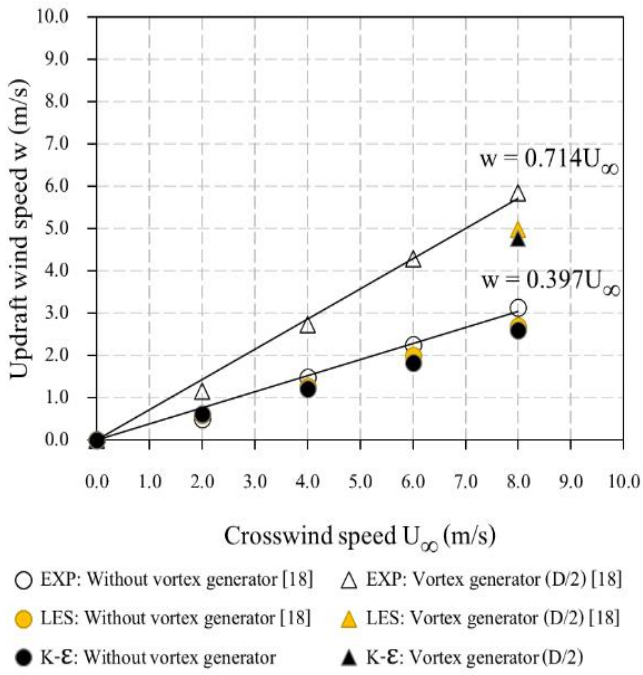

Note: The filled signs showed the result from the numerical model, while the lined signs showed the result gathered from the experiment.

Figure 9. The updraft windspeed in the cylindrical tower

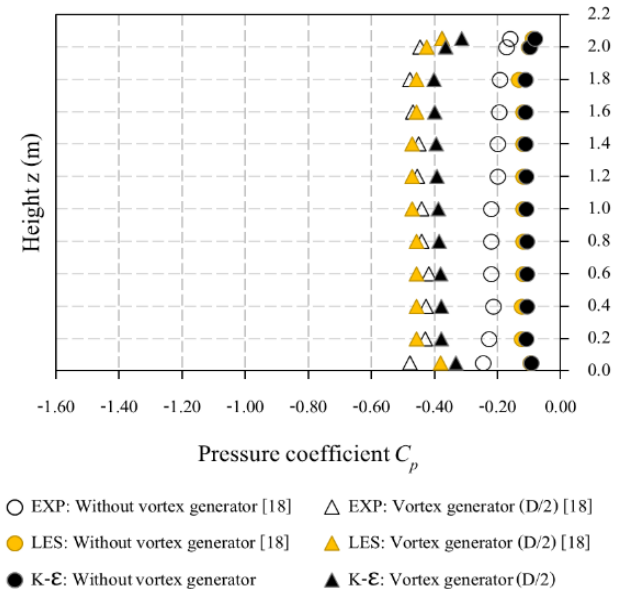

Note: The filled signs showed the result from the numerical model, while the lined signs showed the result gathered from the experiment.

Figure 10. The pressure coefficient of the cylindrical tower

3.2 Numerical results of the updraft windspeed inside the cylindrical tower

Comparisons between the updraft windspeed inside the cylindrical tower without any vortex generators and with diffuser-shaped vortex generators at any angle are displayed in Figures 11-14. The results from those comparisons showed that the 2° diffuser-shaped vortex generators at the heights (h_{vg}) of *D/2*, *D*, and *2D* can enhance 24%, 43%, and 64% of the updraft windspeed, respectively. The 4° diffuser-shaped vortex generator at the heights of *D/2*, *D*, and *2D* can enhance 26%, 46%, and 71% of the updraft windspeed, while the 6° diffuser-shaped generator at the heights of *D/2*, *D*, and *2D* can enhance 27%, 49%, and 75%, respectively. The 8° diffuser-shaped vortex generator at the heights of *D/2*, *D*, and *2D* can enhance 28%, 53%, and 81% of the updraft windspeed, making the 8° diffuser-shaped vortex generator at the heights of *2D* the most suitable vortex generator to install with the cylindrical tower. Results also showed that the higher updraft windspeed enhancement was expected to be seen when the diffuser angle was increasing.

Table 1. The increasing rate of the updraft windspeed of the tower with the diffuser-shaped vortex generators

Types of Three-Directional Vortex Generators	Height (hvg)	Section Area (m^2)	Average Updraft Windspeed Increasing Rate (w)
Without VG	-	-	0.316 *U*∞
Angle of 2°	*D/2*	0.0289	0.387 *U*∞
Angle of 4°	*D/2*	0.0294	0.395 *U*∞
Angle of 6°	*D/2*	0.0299	0.399 *U*∞
Angle of 8°	*D/2*	0.0304	0.404 *U*∞
Angle of 2°	*D*	0.0588	0.446 *U*∞
Angle of 4°	*D*	0.0607	0.459 *U*∞
Angle of 6°	*D*	0.0627	0.469 *U*∞
Angle of 8°	*D*	0.0648	0.481 *U*∞
Angle of 2°	*2D*	0.1214	0.514 *U*∞
Angle of 4°	*2D*	0.1291	0.535 *U*∞
Angle of 6°	*2D*	0.1370	0.551 *U*∞
Angle of 8°	*2D*	0.1451	0.567 *U*∞

From Table 1, it can be observed that the increase in cross-sectional area is directly proportional to the significant increase in updraft velocity.

3.3 Numerical results of the pressure coefficient inside the cylindrical tower

Comparisons between the pressure coefficient inside the cylindrical tower without any vortex generators and with diffuser-shaped vortex generators at any angle at the 8 m/s crosswind are displayed in Figures 15-18. The tower with the generator can provide better low-air pressure than the tower without the generator. In other words, the tower with the generator can provide low air pressure throughout the tower, with the updraft windspeed inside the tower increased due to the lower pressure coefficient. This led to a better suction updraft, and the suction updraft was seen to be improved in the tower with the generator at the h_{vg} heights of *D/2*, *D*, and *2D* respectively.

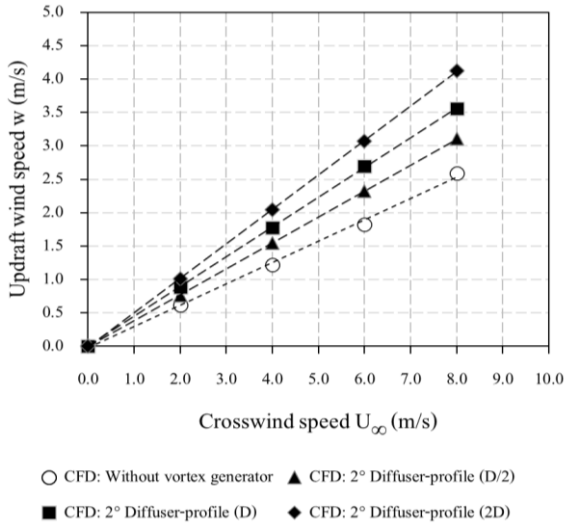

Figure 11. The comparison of updraft windspeed generated from the cylindrical tower without the generator and with a 2° Diffuser-shaped vortex generator

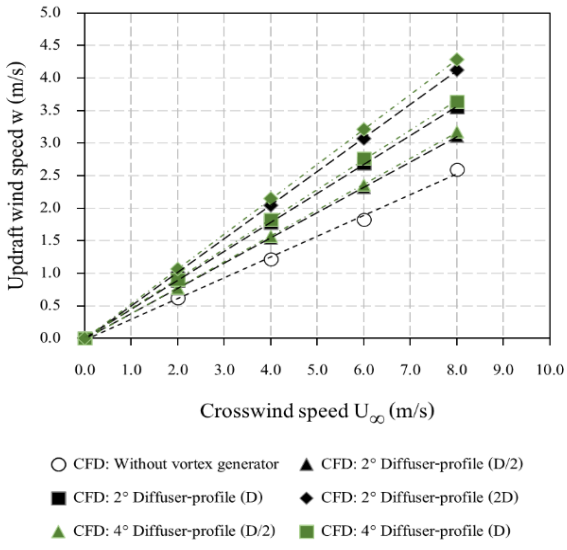

Figure 12. The comparison of updraft windspeed generated from the cylindrical tower without the generator and with a 4° Diffuser-shaped vortex generator

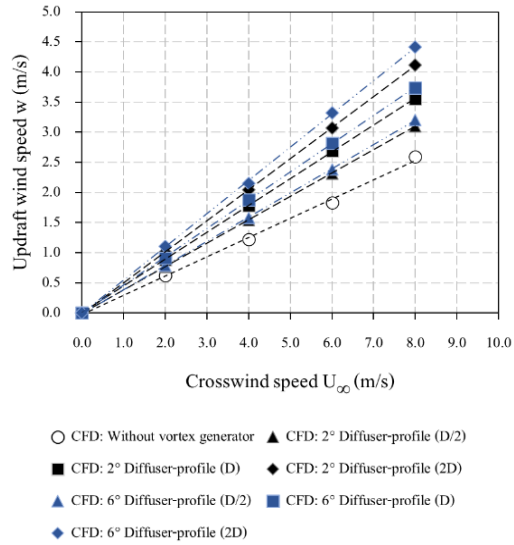

Figure 13. The comparison of updraft windspeed generated from the cylindrical tower without the generator and with a 6° Diffuser-shaped vortex generator

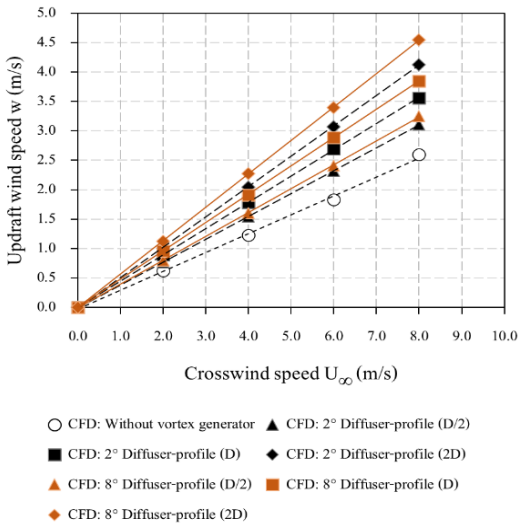

Figure 14. The comparison of updraft windspeed generated from the cylindrical tower without the generator and with an 8° Diffuser-shaped vortex generator

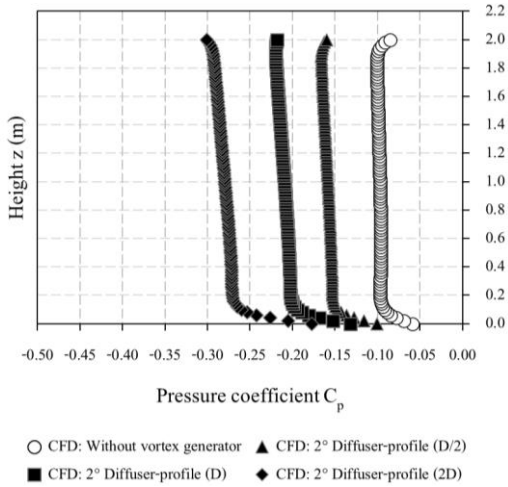

Figure 15. The comparison of the pressure coefficient generated from the cylindrical tower without the generator and with a 2° Diffuser-shaped vortex generator

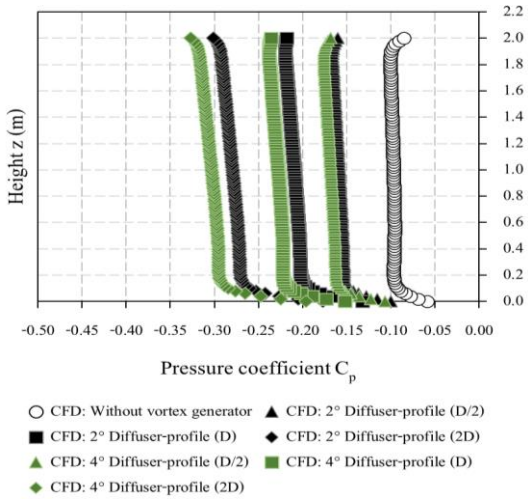

Figure 16. The comparison of the pressure coefficient generated from the cylindrical tower without the generator and with a 4° Diffuser-shaped vortex generator

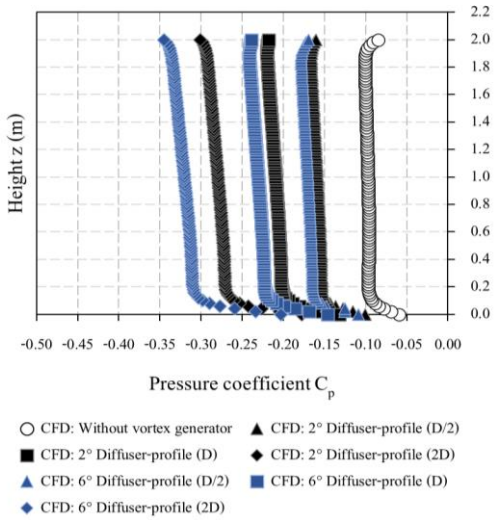

Figure 17. The comparison of the pressure coefficient generated from the cylindrical tower without the generator and with a 6° Diffuser-shaped vortex generator

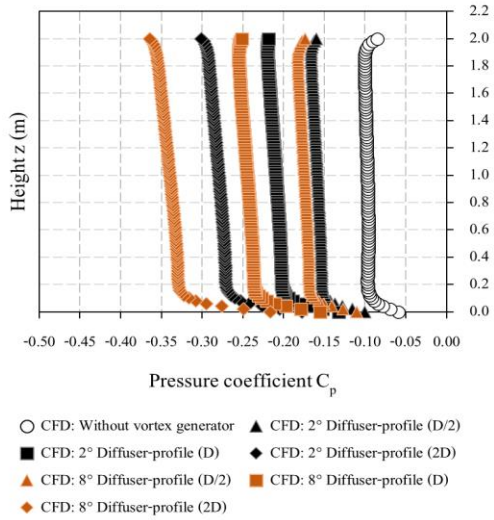

Figure 18. The comparison of the pressure coefficient generated from the cylindrical tower without the generator and with an 8° Diffuser-shaped vortex generator

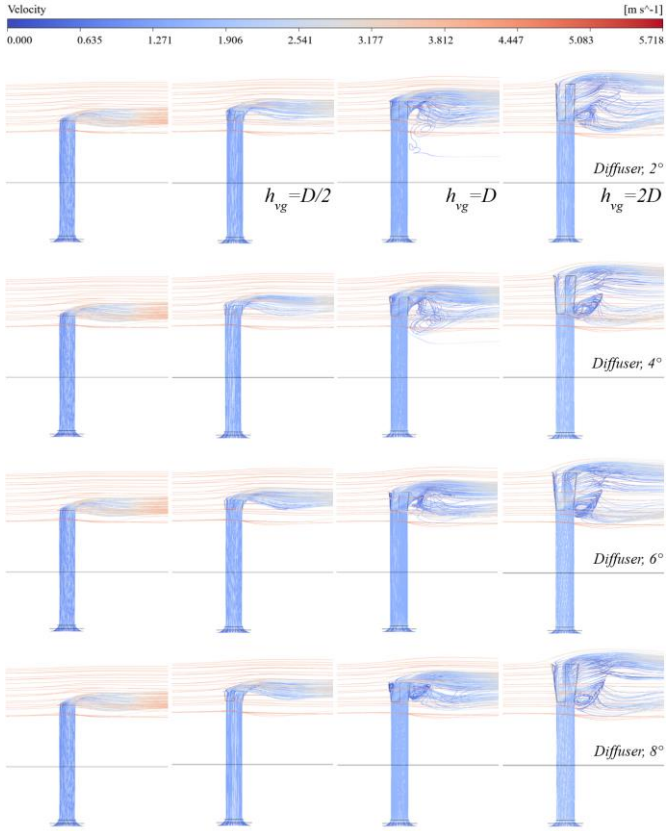

Figure 19. A numerical model of the streamline detected at the tower without the vortex generator and with the different-shaped generators at the 4 m/s crosswind speed

Therefore, this can be said that the pressure coefficient had a relative relationship with the updraft windspeed, which means that the diffuser-shaped vortex generator that improves the updraft windspeed can be better in lowering the pressure coefficient. The reason for the phenomenon was caused by the crosswind that flowed to the generator. It led to a mass of vortex at the outlet that caused the lower pressure throughout the tower, as well as the improved suction updraft, shown in Figure 19. At the generator's height of 0.2 m, the coefficient started to be stable before increasing at the outlet that had the generator installed, making this height suitable for installing the ventilator or electric production fans.

4. STREAMLINE AND PRESSURE COEFFICIENT PATTERNS ON EACH VORTEX GENERATOR

The streamline generated from the numerical model of the cylindrical tower without the generator and with diffuser-shaped vortex generators at different angles at a crosswind speed of 4 m/s is displayed in Figure 18, with the velocity displayed in red lines, and the updraft windspeed displayed in blue lines. According to the streamline model, the crosswind at the outlet caused the suction updraft to be drawn to the tower outlet. The vortex generator, meanwhile, helped add space between the crosswind and the outlet, leading to a better suction updraft. Visible vortex was seen with the tower that installed the 8° diffuser-shaped vortex generator at *D* and *2D* heights due to a better suction updraft, while the generators at *D/2* did not see any but the twisted streamline. Regarding the vortex shape, the vortex started to be seen in the tower with the 2° diffuser-shaped vortex generator at the *D* height,

showing the vortex happening lower than the outlet, and a similar phenomenon was also seen in the *2D* height generator. More visible vortexes were seen while using the 4° diffuser-shaped vortex generator. More visibilities of the vortex and heights of the vortex from the outlet were supposed to be seen when the semi-open angle at 6° and 8°, at the height at *D* and *2D*.

As shown in a pressure coefficient pattern in Figure 19, it can be seen that the vortex, seen as a blue-colored area, was denser at the outlet due to lower pressure and appeared in a darker shade in the pattern when the pressure became even lower. The blue-colored area can also be seen throughout the tower with the vortex generator due to the lower pressure coefficient compared with the tower without it. The tower with the generator at *D/2* height had a wider suction updraft than the tower without it, and the pressure tended to be lower when the generator heights became higher at *D* and *2D*. The pressure was also lower when the semi-open angle became higher, and the coefficient became stable at every crosswind velocity. The observation on the tower with the *2D*-height vortex generator also showed that the lowest coefficient at the generator base was due to the wind plates' widened shape at the base, as seen in Figure 20.

The results also showed that the updraft windspeed increase was related to the height of the vortex generator. due to its increasing wind-receiving surface area, led to a lesser impact of wind at the outlet. The higher vortex generator led to better updraft fluidity to the outlet because of the width difference between the generator base and tip, in a similar fashion to the results [9], which led to better updraft windspeed.

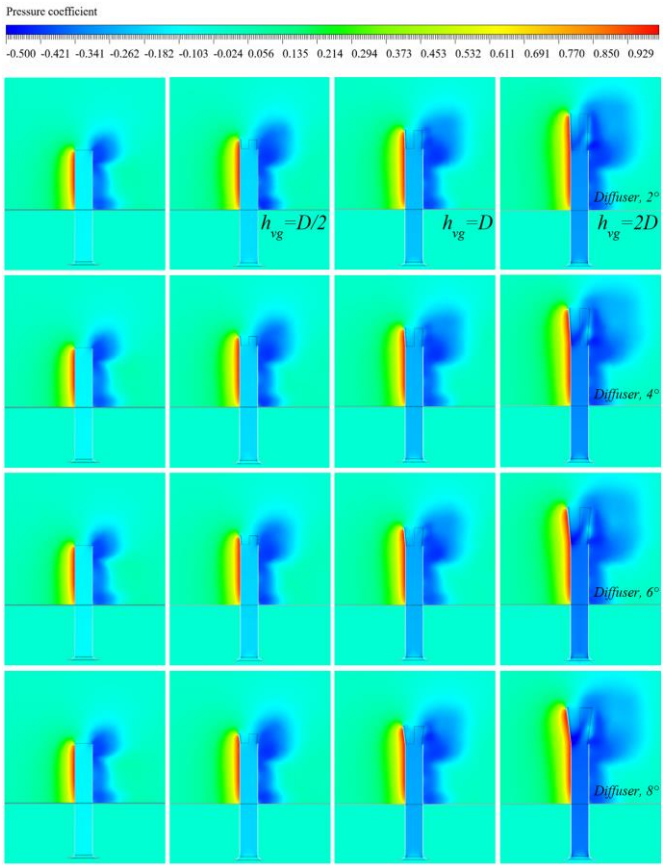

Figure 20. An example of the pressure coefficient that can be seen at the measurement spots of towers without the vortex generator and with the different shaped generators at the 4 m/s crosswind speed

5. CONCLUSION

Developed from the experiment on a single square-plated vortex generator [18], this study focused on developing three-dimensional diffuser-shaped vortex generators that worked by using crosswind energy to generate vortex at the cylindrical tower outlet. The vortex was caused by the lower air pressure, which led to a better suction updraft that led to a better updraft windspeed. The diffuser-shaped generator led to a lower surface area and updraft windspeed. However, it led to maximized wind-receiving ability and more stable installation. The following can be observed in the discussion:

(1) The diffuser-shaped vortex generator at *2D* height can maximize the updraft windspeed the most.

(2) The diffuser-shaped vortex generator and *2D* can maximize the most visible vortex at the outlet, with the vortex in a smaller size can also be seen at the 8° diffuser-shaped vortex generator.

(3) The most suitable for the three-dimensional diffuser wind plates were at 8°, with at least 81% of the updraft windspeed being enhanced.

(4) The updraft windspeed increased when the semi-open angle becomes higher, and the semi-open angle can be increased to be higher than 8° used in this study.

(5) An increase in cross-sectional area is directly proportional to the significant increase in updraft velocity, which is inversely proportional to the decrease in pressure coefficient.

The idea of using crosswind energy to save energy used for cylindrical tower ventilation systems is interesting and open for further development in the following discussions. The suggestions for those would be to focus on the various heights of the diffuser-shaped vortex generator that are related to the diffuser angles, which can lead to a system that can be installed in limited spaces and is most valuable in cost as well. However, further studies are needed on vortex generators with larger half-open angles and the effects of three-directional wind-catching plates. Additionally, the impact of varying ratios when these are installed on towers of different sizes may affect the updraft velocity. Wind tunnel testing is also essential to validate the results obtained from numerical simulations.

Furthermore, for practical applications, the structural integrity of the tower must be considered. Excessive half-open angles and heights of the vortex generators could directly affect the strength of the tower. The selection of the appropriate number of directions for the wind-catching plates, tailored to the seasonal winds of the specific terrain, is also crucial, as this influences the determination of the optimal plate width for achieving the best updraft performance.

REFERENCES

[1] Haaf, W., Friedrich, K., Mayr, G., Schlaich, J. (1983). Solar chimneys part I: Principle and construction of the pilot plant in Manzanares. International Journal of Solar Energy, 2(1): 3-20. http://doi.org/10.1080/01425918308909911

[2] Haaf, W. (1984). Solar chimneys: Part II: Preliminary test results from the Manzanares pilot plant. International Journal of Sustainable Energy, 2(2): 141-161. http://doi.org/10.1080/01425918408909921

[3] Prtetorius, J.P., Kröger, D.G. (2009). The influence of environment on solar chimney power plant performance.

R&D Journal, 25: 2-9. https://www.researchgate.net/publication/385490192_The_Influence_of_Environment_on_Solar_Chimney_Power_Plant_Performance.
[4] Ming, T., Wang, X., de Richter, R.K., Liu, W., Wu, T., Pan, Y. (2012). Numerical analysis on the influence of ambient crosswind on the performance of solar updraft power plant system. Renewable and Sustainable Energy Reviews, 16(8): 5567-5583. https://doi.org/10.1016/j.rser.2012.04.055
[5] Shen, W., Ming, T., Ding, Y., Wu, Y. (2014). Numerical analysis on an industrial-scaled solar updraft power plant system with ambient crosswind. Renewable Energy, 68: 662-676. https://doi.org/10.1016/j.renene.2014.03.011
[6] Silva, J.O.C., Machado, D.S.S., Silva, J.A.D., Maia, C.B. (2017). Numerical determination of the coefficient of heat transfer by convection between coverage and external environment in a small solar chimney. In 24th ABCM International Congress of Mechanical Engineering, Curitiba, Brazil. https://www.researchgate.net/publication/323207327_Numerical_Determination_of_the_Coefficient_of_Heat_Transfer_by_Convection_between_Coverage_and_External_Environment_in_a_Small_Solar_Chimney.
[7] Silva, J.O.C., Gonçalves, L.P., Ledo, L.F.R., Maia, C.B., Hanriot, S.M., Landre, J. (2016). Numerical analysis of the crosswind in small solar chimney. In Proceedings of the 12th International Conference on Heat Transfer, Fluid Mechanics and Thermodynamics, Malaga, Spain, pp. 301-307.
[8] Jafarifar, N., Behzadi, M.M., Yaghini, M. (2019). The effect of strong ambient winds on the efficiency of solar updraft power towers: A numerical case study for Orkney. Renewable Energy, 136: 937-944. https://doi.org/10.1016/j.renene.2019.01.058
[9] Ohya, Y., Wataka, M., Watanabe, K., Uchida, T. (2016). Laboratory experiment and numerical analysis of a new type of solar tower efficiently generating a thermal updraft. Energies, 9(12): 1077. https://doi.org/10.3390/en9121077
[10] Ridwan, A., Hafizh, H., Fauzi, M.R. (2018). Design and experimental test for solar chimney power plant: Case study in Riau Province, Indonesia. IOP Conference Series: Materials Science and Engineering, 403(1): 012092. https://doi.org/10.1088/1757-899X/403/1/012092
[11] Ohya, Y., Karasudani, T. (2010). A shrouded wind turbine generating high output power with wind-lens technology. Energies, 3(4): 634-649. https://doi.org/10.3390/en3040634
[12] Ohya, Y., Karasudani, T., Nagai, T., Watanabe, K. (2017). Wind lens technology and its application to wind and water turbine and beyond. Renewable Energy and Environmental Sustainability, 2: 2. https://doi.org/10.1051/rees/2016022
[13] Kulkarni, S., Badhe, A., Kumbhar, P., Panaval, P., Jadhao, R. (2019). Experimental validation of computational design of wind turbine with wind lens. International Research Journal of Engineering and Technology, 6(2): 1606-1609. https://doi.org/10.14445/23488360/IJME-V6I5P102
[14] Prasad, K.R., Kumar, V.M., Swaminathan, G., Loganathan, G.B. (2020). Computational investigation and design optimization of a duct augmented wind turbine (DAWT). Materials Today: Proceedings, 22: 1186-1191. https://doi.org/10.1016/j.matpr.2019.12.116
[15] Shun, S., Ahmed, N.A. (2012). Wind turbine performance improvements using active flow control techniques. Procedia Engineering, 49: 83-91. https://doi.org/10.1016/j.proeng.2012.10.115
[16] Zhao, Z., Jiang, R., Feng, J., Liu, H., Wang, T., Shen, W., Wang, D., Liu, Y. (2022). Researches on vortex generators applied to wind turbines: A review. Ocean Engineering, 253: 111266. https://doi.org/10.1016/j.oceaneng.2022.111266
[17] Watanabe, K., Ohya, Y. (2021). A simple theory and performance prediction for a shrouded wind turbine with a brimmed diffuser. Energies, 14(12): 3661. https://doi.org/10.3390/en14123661
[18] Watanabe, K., Fukutomi, S., Ohya, Y., Uchida, T. (2020). An ignored wind generates more electricity: A solar updraft tower to a wind solar tower. International Journal of Photoenergy, 2020(1): 4065359. https://doi.org/10.1155/2020/4065359
[19] Boonloi, A., Sudsanguan, A., Jedsadaratanachai, W. (2024). Design and development of vortex generators on cylindrical tower. Modelling and Simulation in Engineering, 2024(1): 3799402. https://doi.org/10.1155/2024/3799402
[20] Boonloi, A., Sudsanguan, A., Jedsadaratanachai, W. (2024). Crosswind and vortex usages for electricity production enhancement of solar updraft tower. Modelling and Simulation in Engineering, 2024(1): 4970781. https://doi.org/10.1155/2024/4970781
[21] Launder, B.E., Spalding, D.B. (1983). The numerical computation of turbulent flows. In Numerical Prediction of Flow, Heat Transfer, Turbulence and Combustion, Pergamon, pp. 96-116. https://doi.org/10.1016/B978-0-08-030937-8.50016-7
[22] Hosder, S., Grossman, B., Haftka, R., Mason, W., Watson, L. (2002). Observations on CFD simulation uncertainties. In 9th AIAA/ISSMO Symposium on Multidisciplinary Analysis and Optimization, p. 5531. https://doi.org/10.2514/6.2002-5531
[23] Tucker, P.G., Rumsey, C.L., Spalart, P.R., Bartels, R.E., Biedron, R.T. (2005). Computations of wall distances based on differential equations. AIAA Journal, 43(3): 539-549. https://doi.org/10.2514/1.8626
[24] Salim, S.M., Cheah, S. (2009). Wall Y strategy for dealing with wall-bounded turbulent flows. In Proceedings of the International Multiconference of Engineers and Computer Scientists, pp. 2165-2170.
[25] Gok, K., Inal, S., Gok, A., Gulbandilar, E. (2017). Comparison of effects of different screw materials in the triangle fixation of femoral neck fractures. Journal of Materials Science: Materials in Medicine, 28: 1-7. https://doi.org/10.1007/s10856-017-5890-y
[26] Fatchurrohman, N., Chia, S.T. (2017). Performance of hybrid nano-micro reinforced mg metal matrix composites brake calliper: Simulation approach. IOP Conference Series: Materials Science and Engineering, 257(1): 012060. https://doi.org/10.1088/1757-899X/257/1/012060

NOMENCLATURE

h_{vg} height of the vortex generators, m

D	diameter of cylindrical tower, m
w	updraft speed, m.s^{-1}
ΔP_s	static pressure difference, kg.m^{-2}
C_p	pressure coefficient
U_∞	flow velocity of crosswind, m.s^{-1}
p	static pressure at the evaluated point, kg.m^{-2}
p_∞	static pressure in the freestream, kg.m^{-2}
k	specific turbulent kinetic energy, m^2.s^{-2}
u_i	incident free-stream airflow, m.s^{-1}
P_k	production of turbulent kinetic energy
P_b	production of turbulent kinetic energy due to buoyancy
S_k	user-defined source
$C_{1\varepsilon}$	constants in the conventional k-epsilon
$C_{2\varepsilon}$	constants in the conventional k-epsilon
$C_{3\varepsilon}$	constants in the conventional k-epsilon

Greek symbols

ρ	fluid density, kg.m^{-3}
μ_t	turbulent or eddy viscosity, kg m^{-1}.s^{-1}
σ_k	constants in the conventional k-epsilon
σ_ε	constants in the conventional k-epsilon
ε	dynamic viscosity, kg.m^{-1}.s^{-1}

Subscripts

CFD	computational fluid dynamics
LES	large eddy simulation
EXP	experiment
VG	vortex generator